

# **Pd/CeO<sub>2</sub> Catalysts as Powder in a Fixed-bed Reactor and as Coating in a Stacked Foil Microreactor for the Methanol Synthesis**

Xuyen Kim Phan<sup>a,d</sup>, John Walmsley<sup>b</sup>, Hamid Bakhtiary-Davijany<sup>a,e</sup>, Rune Myrstad<sup>b</sup>, Peter Pfeifer<sup>c</sup>, Hilde Venvik<sup>a</sup>, Anders Holmen<sup>a,\*</sup>

<sup>a</sup>Department of Chemical Engineering, Norwegian University of Science & Technology, NO-7491 Trondheim, Norway. <sup>b</sup>SINTEF Materials and Chemistry, NO-7465 Trondheim Norway.

<sup>c</sup>Karlsruhe Institute of Technology, Institute for Micro Process Engineering, D-76344 Eggenstein-Leopoldshafen, Germany. <sup>d</sup>Present address: WellCem, NO-4353 Klepp Stasjon, Norway. <sup>e</sup>Present address: Xodus Group, Lysaker Torg 25, NO-1366 Lysaker, Norway

## **Abstract**

Pd/CeO<sub>2</sub> as a catalyst for methanol synthesis has been studied in a microreactor consisting of 14 structured foils and in a fixed-bed laboratory reactor. Methanol synthesis was carried out at 80 bar and 300 °C with a syngas composition of H<sub>2</sub>/CO/CO<sub>2</sub>/N<sub>2</sub> = 65/25/5/5. It was found that Pd/CeO<sub>2</sub> as a foil coating was more active than the Pd/CeO<sub>2</sub> powder catalyst on a Pd/CeO<sub>2</sub> mass basis, both initially and after stabilization. In order to understand the Pd/CeO<sub>2</sub> catalyst properties, both as a coating on the structured foils and as nanoparticles techniques such as TEM, SEM, XRD and chemisorption were employed to characterize the catalysts before and after reaction experiments. The activity of the Pd/CeO<sub>2</sub> foil coating is substantially better than the Pd/CeO<sub>2</sub>

powder despite significantly higher Pd dispersion of the Pd/CeO<sub>2</sub> powder. This is ascribed to the Pd nanoparticles of the powder catalyst being partly covered by the ceria upon preparation and reduction. This prevents the accessibility of Pd to the gaseous reactants. A higher number of active sites are present initially in both catalysts leading to high initial activity for methane as well as methanol formation. This may be explained by good interfacial contact between Pd and CeO<sub>2</sub> created during preparation and reduction to form sites that are gradually lost under reaction conditions by a combination of sintering/agglomeration and enhanced coverage of the Pd by ceria layers.

## KEYWORDS

Microreactor, methanol synthesis, palladium catalyst, cerium oxide, TEM, XRD

## 1. Introduction

Natural gas represents a global energy resource similar in size to that of crude oil. Approximately 50% of the gas reserves could be considered as “stranded”, i.e. lacking pipelines or other infrastructure for transport directly to the market [1]. 50% of the stranded gas is located off-shore. Exploiting offshore gas presents challenges that possibly could be overcome by offshore conversion to methanol, synthetic gasoline/diesel (Fischer-Tropsch technology) or dimethyl ether (DME), processes that may be referred to as gas-to-liquids (GTL) technology. For offshore GTL, a barge mountable production unit would require compact, efficient, robust, light weight, reliable and safe technologies, whereas existing technology is favored by economy of scale and does not meet the requirements for floating installations.

Microstructured reactors [2-4], in which the reaction occurs in parallel channels or structures of critical dimensions ranging from a few  $\mu\text{m}$  to a few  $\text{mm}$ , may represent an interesting potential for offshore GTL technology. Compared to conventional reactors, the high surface-to-volume ratios resulting from the narrow reaction volumes significantly enhance the heat and mass transfer [5-8]. Highly exothermic reactions may be carried out at nearly isothermal conditions [9, 10] or even with controlled temperature gradients over the reactor [11]. The suppression of hot spots not only results in safe operation, but helps prolonging the lifetime of the catalysts [12, 13]. It may also reduce the extent of undesirable side reactions, leading to higher selectivity [14, 15]. This may again allow for accommodation of catalysts with 1-2 orders of magnitude higher activity than existing technology in certain cases. Eventually, this could lead to increased product yields, improved energy efficiency, smaller process footprints and reduced capital costs [16].

Methanol is one of the basic intermediates in the chemical industry and is also being used as a fuel additive and as a clean burning fuel. It is the starting point for formaldehyde, methyl tert-butyl ether and several solvents [17, 18]. Methanol can also be converted to olefins (ethene, propene, etc.) by recently developed processes [19]. Industrial production of methanol is carried out directly from synthesis gas over a  $\text{CuO}/\text{ZnO}/\text{Al}_2\text{O}_3$  catalyst. The main reactions for the formation of methanol from syngas are:

Methanol synthesis from CO:



Methanol synthesis from  $\text{CO}_2$ :



The two methanol forming reactions are coupled by the water gas shift reaction:



The advantages of the CuO/ZnO/Al<sub>2</sub>O<sub>3</sub> catalyst are many, since it has relatively low cost and high selectivity to methanol, and the system is mature and well-developed. Possible disadvantages include the tendency to sintering at temperatures greater than 270-300 °C [20] and a reaction mechanism that requires carbon dioxide to be present in the feed, resulting in water as a by-product in the reaction. Supported palladium has been suggested as an alternative catalyst because the reaction mechanism proceeds via carbon monoxide [21] and because it is possibly a more active metal than copper. However, reports on the activity and selectivity of Pd catalysts have not been too encouraging when compared to Cu-based catalysts [21-24]. Matsumura et al. have reported that Pd in combination with ceria as support or promoter exhibited higher activity for methanol synthesis from carbon monoxide and hydrogen than the conventional Cu-based catalysts [25, 26]. The high catalytic activity was attributed to the presence of Pd species in the cationic form (close to +1), due to strong interaction between Pd and ceria [27]. Moreover, Pd based catalysts may be an alternative to Cu-based catalyst as they possess better tolerance towards sulphur poisoning [28], which is becoming increasingly important for coal or biomass derived synthesis gas feed.

Arising from the interest in developing offshore GTL technologies, the topic of methanol synthesis in microstructured reactors became part of our research activities. We have previously studied Pd/CeO<sub>2</sub> catalyst as a coating in a stacked foil microreactor for methanol synthesis [29]. The coating was then compared with a CuO/ZnO/Al<sub>2</sub>O<sub>3</sub> coating as well as a Pd/CeO<sub>2</sub> catalyst powder in a fixed-bed reactor. The Pd/CeO<sub>2</sub> coated foils showed higher methanol productivity than that of Cu system on a mole of active metal basis (Pd/Cu), although at higher temperature

and with significantly higher methane by-product formation. In this study, we proceed to obtain more detailed understanding of the Pd/CeO<sub>2</sub> catalysts, both as a coating on the structured foils and as nanoparticles. TEM, SEM, XRD and chemisorption were therefore employed to characterize the catalysts before and after reaction experiments

## 2. Experimental

The stacked foil microreactor (SFMR) consisting of fourteen structured foils (Figure 1) was made by Karlsruhe Institute of Technology (KIT) and the details were given previously [29]. The structured and coated foils were stacked inside a steel (Alloy 800) housing, using graphite seals (Novaform SK, Frentzelit) to allow for high pressure. Two metal blocks, one below and one above the stack, were used to adapt the height of the stack to the housing and thereby ensuring leak tightness and minimal reactant bypass issues. The SFMR was electrically heated by 16 cartridges to maintain a uniform temperature profile, which was recorded by insertion of thermocouples into holes in the SFMR outer shell.

The fixed-bed reactor (FBR) was made of a 1/2" 316 stainless steel tube with an internal diameter of 10 mm. 1 g of catalyst particles (50-120µm) were kept in place by a stainless steel cylinder capped with a steel gauze inserted into the reactor bottom. The catalyst bed length was about 20 mm. The FBR was clamped inside an aluminum block and heated by a Kanthal furnace that was regulated against a thermocouple placed between the reactor and the aluminum block. The catalyst bed temperature was recorded by a movable thermocouple inside a thermowell centered inside the reactor. For comparison between foil and FBR experiments, the furnace temperature was adjusted so that the maximum bed temperature ( $T_{\text{peak}}$ ) along the FBR axis corresponded to the practically isothermal mid-section SFMR temperature [29].

The Pd/CeO<sub>2</sub> foil coating was prepared by dripping a CeO<sub>2</sub> sol-gel, synthesized according to Ozer et al. [30] from cerium ammonium nitrate, uniformly over the microchannels. This was followed by drying at 70 °C overnight and calcination at 500 °C for 5 h in air. The CeO<sub>2</sub> layer was then dripped several times with a PdCl<sub>2</sub> solution (Sigma Aldrich, 5 wt% in 10 wt% HCl solution) until 10 wt% Pd/CeO<sub>2</sub> was obtained, and then dried and calcined as before. The catalyst mass obtained in SFMR is 181.3 mg. For fixed-bed experiments, 50-120 μm particles of a 10%Pd/CeO<sub>2</sub> powder was prepared by deposition – precipitation [25], using CeO<sub>2</sub> nanopowder (Sigma Aldrich, d < 25 nm) and the same PdCl<sub>2</sub> solution as precursors.

The specific surface area ( $S_{\text{BET}}$ ) of all the supports and catalysts was determined by N<sub>2</sub> adsorption at -196 °C using a Micromeritics Tristar 3000 instrument. The samples were filled into the sample tube and outgassed overnight under vacuum at 200 °C before measurements. The specific surface area was calculated by the BET (Brunauer-Emmet-Teller) equation. The total pore volume and pore size distribution were found applying the Barrett-Joyner-Halenda (BJH) method [31].

X-ray diffraction analysis of the CeO<sub>2</sub> support and the Pd/CeO<sub>2</sub> powders was performed on a Bruker AXS D8 Focus with D8 Goniometer, CuK $\alpha$  radiation ( $\lambda=1.54\text{\AA}$ ) and a Lynxeye detector. The XRD patterns were acquired in the  $2\theta$ -range of 20-90° with a step size of 0.03° and a step time of 0.6s. The diffractograms were compared with standards in a database (EVA) for phase identification [32].

Volumetric chemisorption of CO was performed at 313 K on a Micromeritics ASAP 2010C unit. The catalyst was loaded into a U-shaped quartz reactor and placed inside an electric furnace. The sample was initially evacuated at 313 K for one hour, and reduced in flowing hydrogen at 573 K for 16 h. The temperature was increased slowly by 1 K/min. After reduction, the sample was evacuated for 1 hour at 573 K, for 30 min at 373 K and subsequently cooled to 313 K for adsorption measurement. The Pd dispersion (D, %) was calculated assuming that one Pd site was covered by one CO molecule.

High resolution - Inductively coupled plasma – Mass Spectrometry (HR-ICP-MS) was used to determine the actual catalyst composition of the Pd/CeO<sub>2</sub> powder. The analysis was performed by Molab AS. The sample was completely dissolved in a solution of 0.1M HNO<sub>3</sub> and 0.1 vol% HF before analysis.

Scanning electron microscopy (SEM) was performed using a Zeiss Ultra instrument operated at beam voltage of 20 kV. SEM energy-dispersive X-ray spectroscopy (EDS) analysis and mapping was performed using a Bruker Quantex system.

Transmission electron microscopy (TEM) and TEM EDS analysis were performed using a JEOL 2010F instrument, operated at 200 kV, and an Oxford Instruments INCA system, respectively. The TEM samples were prepared by dispersing a small amount of powder in ethanol and placing a drop of the liquid on a carbon support film supported on a copper grid. The grid was dried while resting on a filter paper before being transferred directly to the TEM.

Before reaction experiments, the Pd/CeO<sub>2</sub> catalysts were reduced at atmospheric pressure under 10 vol.% hydrogen in nitrogen at 300 °C. After reduction, the reactors were pressurized up to 80 bar under premixed syngas (H<sub>2</sub>/CO/CO<sub>2</sub>/N<sub>2</sub> = 65/25/5/5). The product gas was analyzed using an Agilent 6890 N GC with TCD and FID detectors set-up for both online feed and product gas analysis as well as offline liquid product analysis. The effluent gas composition was analyzed at regular intervals over approximately 24 h to obtain stable values before the parameters were changed. For comparison of the SFMR and FBR performance, the furnace temperature was adjusted so that the maximum bed temperature (T<sub>peak</sub>) along the FBR axis corresponded to the practically isothermal mid-section SFMR temperature.

The conversion, reaction rates and contact time were calculated based on the composition of feed gas, composition of the effluent gas and the amount of liquid collected, as follows:

$$\text{CO conversion [\%]:} \quad X_{CO} = \frac{n_{CO,in} - n_{CO,out}}{n_{CO,in}} \times 100 \quad (4)$$

$$\text{Rate of methanol formation:} \quad r_{MeOH} = \frac{mmol_{MeOH}}{g_{cat} \cdot h} \quad (5)$$

$$\text{Rate of CH}_4 \text{ by-product formation} \quad r_{CH_4} = \frac{mmol_{CH_4}}{g_{cat} \cdot h} \quad (6)$$

$$\text{Contact time:} \quad W / F = \frac{g_{cat}}{F \left( \frac{Ncm^3_{syngas}}{ms} \right)} \quad (7)$$

The liquid product was assumed to consist of methanol and water only in the mass balance calculations. The validity of this assumption has been checked in selected liquid products. Even if it is evident that evaporation of some of the product takes place under liquid collection and

analysis, the carbon balance is closed within  $\pm 5\%$  using this method. The presence of minor amounts of other oxygenates in the liquid product can not be excluded.

### 3. Results and discussion

#### 3.1. Performance of the Pd/CeO<sub>2</sub> catalysts

As mentioned, the performance of the Pd/CeO<sub>2</sub> catalysts as a powder in FBR and as a coating in SFMR under methanol synthesis conditions has been previously reported in detail [29]. For convenience, the most relevant and conclusive data in terms of activity have been included here. Figure 2a shows conversion and reaction rates at 80 bar, 300 °C and a contact time of 110 ms.g<sub>cat</sub>/cm<sup>3</sup>. The Pd/CeO<sub>2</sub> foil coating and the Pd/CeO<sub>2</sub> powder catalyst show very similar trends in performance, but at different activity levels. The initial activity is high but significant deactivation occurs. The activity of the Pd/CeO<sub>2</sub> foil coating and the Pd/CeO<sub>2</sub> powder catalyst reached a pseudo steady-state after about ~ 120 h and ~ 60h, resulting in a decrease in CO conversion from 65% to 11% and from 32% to 4%, respectively. The deactivation was accompanied with lower rates of methanol as well as methane formation, but was more significant for the methane formation (Figure 2b). The catalysts therefore appear to have a high initial number of sites active in both methanol and methane formation that are unstable and gradually lost during reaction. Both catalysts seem to retain more of the sites that are selective to methanol only. It could be that at least two types of sites exist, on which one is only leading to methanol. The other type(s) could be active for methane formation only, or less selective but prone to deactivation. We also prepared 5 wt% Pd particles supported on ZnO or SiO<sub>2</sub> (not shown) by impregnation, for which the activity was low even during the initial period. Under similar conditions and contact time on a Pd/support mass basis, the CO conversion was only 2-

4%. CeO<sub>2</sub> supported particles were therefore also subjected to the same methanol synthesis reaction conditions, finding that CeO<sub>2</sub> by itself has negligible activity. This indicates that the Pd particles alone do not contain the most active sites for methanol and methane formation. One may infer that the Pd-ceria interface is essential to the product formation [33], possibly in combination with spillover effects.

Pd/CeO<sub>2</sub> as a foil coating is more active than the Pd/CeO<sub>2</sub> powder catalyst on a Pd/CeO<sub>2</sub> mass basis, both initially and after stabilization. Possible differences in performance exist between the two reactor systems, SFMR vs. FBR, but these are found to be minor and related to somewhat different temperature profiles [29]. The main difference must therefore lie in the Pd/CeO<sub>2</sub> composition and structure, as will be discussed below.

### **3.2. Characterization of Pd/CeO<sub>2</sub> powder catalyst**

The BET surface area, pore volume and average pore radius ( $d_{\text{pore}}$ ) of the CeO<sub>2</sub> support and the CeO<sub>2</sub> after loading it with 10 wt% of Pd (fresh Pd/CeO<sub>2</sub> powder) are summarized in Table 1. After Pd deposition, the BET surface area is significantly increased, from 32 to 52 m<sup>2</sup>/g. The average pore radius decreased from 21 to 14 nm, while the pore volume remained more or less the same. The increase in surface area could partly be due to formation of small Pd particles. The pore size distribution of the CeO<sub>2</sub> support and the Pd/CeO<sub>2</sub> powder (Figure 3) shows, however, that the increase in surface area could also be due to a change in the structure of the support, since two new peaks in the pore size distribution appeared at 2.5 and 20 nm. The small peak at 5 nm of the CeO<sub>2</sub> support seems to disappear or becomes hidden because of overlap with the strong new peaks of the Pd/CeO<sub>2</sub>. It should be noted that since PdCl<sub>2</sub> can be dissolved in HCl solution but not in water, 5 wt% PdCl<sub>2</sub> in 10 wt% HCl was used as a precursor. A considerable amount of

HCl was therefore added to the CeO<sub>2</sub> nanopowder solution to reach the loading of 10 wt% Pd. This could possibly have partly dissolved or eroded the CeO<sub>2</sub> crystallites, leading to changes in the structure of the support. However, as shown in Figure 4, the XRD spectra of the CeO<sub>2</sub> support and the fresh Pd/CeO<sub>2</sub> powder look similar and indicate that the CeO<sub>2</sub> phases in both cases were crystalline.

The Pd dispersion of the fresh Pd/CeO<sub>2</sub> catalyst as measured by CO chemisorption was quite high, up to 32%, resulting in an estimated Pd particle size of 3.4 nm (Table 1). Previous studies indicate that the determination of Pd dispersion by CO chemisorption is not straightforward since ceria can chemisorb CO [34, 35] and that the CO adsorption may also be influenced by CeO<sub>2</sub> structure [36]. Pd crystallites could not be detected in the fresh catalyst by XRD (Figure 4), however, in spite of relatively high loading of Pd. This is indirect proof of Pd particles of a few nanometers in size and in line with the chemisorption result.

The morphological properties of the freshly prepared Pd/CeO<sub>2</sub> powder were also investigated by TEM and the results are shown in Figure 5 and 6. From the bright-field TEM images (Figure 5), it can be seen that the Pd/CeO<sub>2</sub> catalyst is composed of agglomerated particles of a few to tens of nanometers in size. It is, however, difficult to identify Pd crystallites even at high resolution, which is probably partly because of electron scattering by CeO<sub>2</sub> [37]. It could also be that the Pd particles are covered by CeO<sub>2</sub> during preparation in HCl and hence less visible in TEM. This could explain the difference in activity between the foil coating and the powder catalyst by significantly lower accessibility of the Pd in the powder by the reactants. Figure 6 shows dark-field STEM micrographs and complementary EDS mapping of Ce, Pd and O in the fresh

Pd/CeO<sub>2</sub> powder. The distribution of the elements (Figure 6b-d) indicates that Pd is well dispersed in/on the CeO<sub>2</sub> support, again in agreement with the existence of Pd nanoparticles.

Figure 7 shows dark-field STEM micrographs and complementary EDS mapping of the Pd/CeO<sub>2</sub> catalyst after about 200 h under methanol synthesis conditions. The Pd remains well dispersed in/on the CeO<sub>2</sub> support for the used Pd/CeO<sub>2</sub> powder, possibly with indications of agglomeration or particle growth. The appearance of a small and broad Pd peak in the XRD spectrum of the used catalyst (Figure 4) supports this, but also indicates that the Pd particles remain small in size. Shen et al. reported strong sintering of Pd during methanol synthesis at 250 °C over 2.44 wt% Pd/CeO<sub>2</sub> during ~30 h on stream, with Pd particles increasing in size from a few nanometers to about hundred nanometers [38]. We have used the same catalyst preparation technique as Shen et al., i.e. deposition-precipitation. The differences are the source of CeO<sub>2</sub> and the relatively higher Pd loading. The application of CeO<sub>2</sub> nanoparticles (< 25 nm) and considerable amounts of HCl as explained above could have influenced the catalyst properties. Strong interaction between the ceria and Pd nanoparticles, or even partly dissolved or eroded CeO<sub>2</sub> creating a layer to partly cover the Pd nanoparticles, could possibly also have prevented agglomeration and sintering of Pd. Then, migration of partly reduced ceria under reaction conditions could further reduce the accessibility of Pd by the reactants [36].

The Pd loading obtained for the Pd/CeO<sub>2</sub> powder, as measured by HR-ICP-MS, is 8.25 wt%. This is less than the nominal loading and possibly less than that of the coating catalyst (both 10 wt% Pd nominally). The reduction in Pd loading was only ~18%, however, while the activity of the powder is less than half compared to that of the coating. In combination with the fact that the powder catalyst has smaller Pd particles than the coating (will be shown below), the lower

relative activity of the powder further supports the existence of (partly reduced) ceria layers that suppress the Pd or Pd-CeO<sub>2</sub> interfacial sites.

### **3.3. Characterization of Pd/CeO<sub>2</sub> as a foil coating**

Figure 8 shows the surface of a microstructured foil coated with Pd/CeO<sub>2</sub> before being used in methanol synthesis experiments as imaged in SEM. It can be seen that the coating layer of Pd/CeO<sub>2</sub> is not completely homogeneous on the foil surface. The high magnification SEM image of Figure 8b reveals that the coating in the middle of the microchannel bottom is relatively homogeneous, but cracks can be found near the corners since a higher catalyst mass is usually obtained in the corner. This is common when using a flow coating technique, since the adhesion to the channel walls is stronger and less of the residual coating liquid will be removed by pressurized air flow.

Figure 9 compares SEM images of the PdCeO<sub>2</sub> coating before and after about 400h under methanol synthesis conditions. Pd particles (white) can be seen at both low and high magnification. EDS proves that the Pd peak is not present in areas away from the white particles, indicating that Pd is not there. For the fresh coated foil (Figure 9a-b), the Pd particles vary in size from tens to about one hundred nanometers, and the Pd particles appear to be round and compact sitting on top of the CeO<sub>2</sub> coating. This could imply that the higher activity of the foil coating relative to that of the powder catalyst is explained by all Pd particles being accessible to the reacting gases, despite being considerably larger in size. For the used coated foil, the Pd particles appear larger in size, almost up to 1 μm (Figure 9c-d). But they also appear less compact and more as agglomerated clusters spread out over the support surface. The interfacial contact between Pd and support hence appears stronger in the used foil coating. As mentioned, ceria may be reduced under reduction and methanol reaction conditions [36], with the possibility of

partially reduced species migrating to/between the Pd crystallites. While this is probably associated with the deactivation observed, it could also contribute to the formation of a strong metal-support interaction and increasing interfacial contact that eventually stabilizes the larger Pd particles of the foil coating.

#### **4. Conclusion**

A Pd/CeO<sub>2</sub> catalyst foil coating to produce methanol from synthesis gas was prepared for application in a stacked foil microstructured reactor (SFMR), and comparison to Pd/CeO<sub>2</sub> powder catalyst fixed-bed experiments was made to better understand its properties. Both Pd/CeO<sub>2</sub> catalysts show high initial activity in SFMR and FBR, respectively, but deactivate significantly to reach steady state after 60-120 hours on the stream. The high initial activity could be due to that active sites at the interfacial contact between Pd and CeO<sub>2</sub> during reduction are gradually lost. Since the loss can not be fully explained by sintering/agglomeration, particularly for the powder catalyst, it is ascribed to migration of partly reduced ceria under reaction condition. The activity of the Pd/CeO<sub>2</sub> foil coating prepared via a sol-gel procedure is substantially better than the Pd/CeO<sub>2</sub> particles prepared by deposition-precipitation onto CeO<sub>2</sub> nanoparticles, initially as well as after stabilization, although the Pd/CeO<sub>2</sub> powder has higher Pd dispersion. This is ascribed to the Pd nanoparticles being covered by a ceria under the preparation and subsequent reduction. This maintains most of the Pd sites covered and inactive in the methanol synthesis. Similar phenomena seem to occur also in the foil coating, but because of the preparation results in larger Pd particles residing on top of a ceria layer, the Pd or Pd-CeO<sub>2</sub> interface remains more accessible to the reactants.

## **Acknowledgements**

The Enabling Production of Remote Gas project performed under the strategic Norwegian Research program PETROMAKS. The authors acknowledge the partners; Statoil ASA, UOP, Bayerngas Norge, Aker Solutions, DNV, and the Research Council of Norway (168223/S30) for support. H.J. Venvik would like to acknowledge the financing by Statoil ASA through the Gas Technology Centre (NTNU-SINTEF) ([www.ntnu.no/gass/](http://www.ntnu.no/gass/)).

## References

1. *Syntroleum to Build Barge-mounted Gas-To-Liquids Plants*. Business Journal, Worldwide Energy, 2003. **Oct 1**.
2. W. Bier, W. Keller, G. Linder, D. Seidel, and K. Schubert, *Manufacturing and testing of compact micro heat-exchanger with high volumetric heat transfer coefficients*. Symp. Vol. DSC, 1990. **ASME(19)**: p. 189-197.
3. A. Holmen, H.J. Venvik, R. Myrstad, J. Zhu, and D. Chen, *Monolithic, microchannel and carbon nanofibers/carbon felt reactors for syngas conversion by Fischer-Tropsch synthesis*. Catalysis Today, 2013. **216**: p. 150-157.
4. J. Yang, S.B. Eiras, R. Myrstad, H.J. Venvik, P. Pfeifer, and A. Holmen, *Fischer-Tropsch synthesis over high-loading Co-based catalysts in a microchannel reactor*. ACS Book K15363, Ch 12. Vol. 284. in Press.
5. M.W. Losey, M.A. Schmidt, and K.F. Jensen, *Microfabricated Multiphase Packed-Bed Reactors: Characterization of Mass Transfer and Reactions*. Ind. Eng. Chem. Res., 2001. **40(12)**: p. 2555-2562.
6. S. Taghavi-Moghadam, A. Kleemann, and G. Golbig, *Microreaction Technology as a Novel Approach to Drug Design, Process Development and Reliability*. Org. Process Res. Dev., 2001. **5(6)**: p. 652-658.
7. V. Hessel, S. Hardt, and H. Löwe, *Chemical Micro Process Engineering: Fundamentals, Modelling and Reactions*; Wiley: Weinheim. 2004.
8. W. Ehrfeld, V. Hessel, and H. Löwe, *Microreactors - New Technology for Modern Chemistry*; Wiley: Weinheim. 2000.
9. H. Bakhtiary-Davijany, F. Hayer, X.K. Phan, R. Myrstad, H.J. Venvik, P. Pfeifer, and A. Holmen, *Characteristics of an Integrated Micro Packed Bed Reactor-Heat Exchanger for methanol synthesis from syngas*. Chem. Eng. J., 2011. **167(2-3)**: p. 496-503.
10. R. Myrstad, S. Eri, P. Pfeifer, E. Rytter, and A. Holmen, *Fischer-Tropsch synthesis in a microstructured reactor*. Catal. Today, 2009. **147(Supplement 1)**: p. S301-S304.
11. P. Pfeifer, K. Haas-Santo, J. Thormann, and K. Schubert, *One pass synthesis of pure sulphur trioxide in microreactors*. Chem. Oggi, 2007. **2**: p. 42-46.

12. I. Aartun, H.J. Venvik, A. Holmen, P. Pfeifer, O. Görke, and K. Schubert, *Temperature profiles and residence time effects during catalytic partial oxidation and oxidative steam reforming of propane in metallic microchannel reactors*. Catal. Today, 2005. **110**(1-2): p. 98-107.
13. I. Aartun, B. Silberova, H. Venvik, P. Pfeifer, O. Görke, K. Schubert, and A. Holmen, *Hydrogen production from propane in Rh-impregnated metallic microchannel reactors and alumina foams*. Catal. Today, 2005. **105**(3-4): p. 469-478.
14. J. Yoshida, A. Nagaki, T. Iwasaki, and S. Suga, *Enhancement of Chemical Selectivity by Microreactors*. Chem. Eng. Technol., 2005. **28**(3): p. 259-266.
15. O. De la Iglesia, V. Sebastián, R. Mallada, G. Nikolaidis, J. Coronas, G. Kolb, R. Zapf, V. Hessel, and J. Santamaría, *Preparation of Pt/ZSM-5 films on stainless steel microreactors*. Catal. Today, 2007. **125**(1-2): p. 2-10.
16. *The microchannel revolution*. Focus Catal., 2005(2): p. 1-2.
17. S. Lee, *Methanol Synthesis Technology*, CRC Press: Florida. 1990.
18. E. Fiedler, G. Grossmann, D.B. Kersebohm, G. Weiss, and C. Witte, *Methanol*. Ullmann's Encyclopedia of Industrial Chemistry. 2000: Wiley-VCH Verlag GmbH & Co. KGaA.
19. T. Mokrani and M. Scurrill, *Gas Conversion to Liquid Fuels and Chemicals: The Methanol Route-Catalysis and Processes Development*. Catal. Rev. - Sci. Eng., 2009. **51**(1): p. 1 - 145.
20. M. Kurtz, H. Wilmer, T. Genger, O. Hinrichsen, and M. Muhler, *Deactivation of Supported Copper Catalysts for Methanol Synthesis*. Catal. Lett., 2003. **86**(1): p. 77-80.
21. M.L. Poutsma, L.F. Elek, P.A. Ibarbia, A.P. Risch, and J.A. Rabo, *Selective formation of methanol from synthesis gas over palladium catalysts*. J. Catal., 1978. **52**(1): p. 157-168.
22. G.C. Chinchin, P.J. Denny, J.R. Jennings, M.S. Spencer, and K.C. Waugh, *Synthesis of Methanol: Part 1. Catalysts and Kinetics*. Appl. Catal., 1988. **36**: p. 1-65.
23. C. Sudhakar and M.A. Vannice, *Methanol and methane formation over palladium/rare earth oxide catalysts*. J. Catal., 1985. **95**(1): p. 227-243.
24. L. Fan and K. Fujimoto, *Promotive SMSI Effect for Hydrogenation of Carbon Dioxide to Methanol on a Pd/CeO<sub>2</sub> Catalyst*. J. Catal., 1994. **150**(1): p. 217-220.

25. W.J. Shen, Y. Ichihashi, M. Okumura, and Y. Matsumura, *Methanol synthesis from carbon monoxide and hydrogen catalyzed over Pd/CeO<sub>2</sub> prepared by the deposition-precipitation method*. Catal. Lett., 2000. **64**(1): p. 23-25.
26. W.-J. Shen, Y. Ichihashi, and Y. Matsumura, *A Comparative Study of Palladium and Copper Catalysts in Methanol Synthesis*. Catal. Lett., 2002. **79**(1): p. 125-127.
27. Y. Matsumura, W.-J. Shen, Y. Ichihashi, and M. Okumura, *Low-Temperature Methanol Synthesis Catalyzed over Ultrafine Palladium Particles Supported on Cerium Oxide*. J. Catal., 2001. **197**(2): p. 267-272.
28. Y. Ma, Q. Ge, W. Li, and H. Xu, *A sulfur-tolerant Pd/CeO<sub>2</sub> catalyst for methanol synthesis from syngas*. J. Nat. Gas Chem., 2008. **17**(4): p. 387-390.
29. X.K. Phan, H.D. Bakhtiary, R. Myrstad, J. Thormann, P. Pfeifer, H.J. Venvik, and A. Holmen, *Preparation and Performance of a Catalyst-Coated Stacked Foil Microreactor for the Methanol Synthesis*. Ind. Eng. Chem. Res., 2010. **49**(21): p. 10934-10941.
30. N. Ozer, J.P. Cronin, and S. Akyuz. *Electrochromic performance of sol-gel-deposited CeO<sub>2</sub> films*. in *Switchable Materials and Flat Panel Displays*. 1999. Denver, CO, USA: SPIE.
31. E.P. Barrett, L.G. Joyner, and P.P. Halenda, *The Determination of Pore Volume and Area Distributions in Porous Substances. I. Computations from Nitrogen Isotherms*. J. Am. Chem. Soc., 1951. **73**(1): p. 373-380.
32. J.W. Niemantsverdriet, *X-Ray Diffraction, Spectroscopy in Catalysis, an Introduction*. Wiley-VCH, 2000: p. 138-145.
33. S. Naito, S. Aida, T. Kasahara, and T. Miyao, *Infrared spectroscopic study on the reaction mechanism of CO hydrogenation over Pd/CeO<sub>2</sub>*. Res. Chem. Intermed., 2006. **32**(3): p. 279-290.
34. A. Trovarelli, G. Dolcetti, C. de Leitenburg, J. Kaspar, P. Finetti, and A. Santoni, *Rh-CeO<sub>2</sub> interaction induced by high-temperature reduction. Characterization and catalytic behaviour in transient and continuous conditions*. J. Chem. Soc., Faraday Trans., 1992. **88**(9): p. 1311-1319.
35. A. Guerrero-Ruiz, S. Yang, Q. Xin, A. Maroto-Valiente, M. Benito-Gonzalez, and I. Rodriguez-Ramos, *Comparative Study by Infrared Spectroscopy and Microcalorimetry of*

- the CO Adsorption over Supported Palladium Catalysts*. Langmuir, 2000. **16**(21): p. 8100-8106.
36. A. Trovarelli, *Catalytic Properties of Ceria and CeO<sub>2</sub>-Containing Materials*. Catal. Rev. - Sci. Eng., 1996. **38**(4): p. 439 - 520.
37. L. Kepinski, M. Wolcyrz, and J. Okal, *Effect of chlorine on microstructure and activity of Pd/CeO<sub>2</sub> catalysts*. J. Chem. Soc., Faraday Trans., 1995. **91**(3): p. 507-515.
38. W.-J. Shen, A. Kobayashi, Y. Ichihashi, Y. Matsumura, and M. Haruta, *Growth of Pd particles in methanol synthesis over Pd/CeO<sub>2</sub>*. Catal. Lett., 2001. **73**(2): p. 161-165.

## Figure Captions

**Figure 1** Pictures of the stacked foil microreactor (SFMR) under operation (a), opened (b).

**Figure 2** CO conversion and rate of methanol (a) and methane by-product (b) formation as a function of time on stream (TOS) for Pd/CeO<sub>2</sub> catalysts as a powder in FBR and as a foil coating in SFMR. T = 300 °C, contact time W/F = 110 [ms·g<sub>cat</sub>/cm<sup>3</sup>], pressure 80 bar and syngas composition H<sub>2</sub>/CO/CO<sub>2</sub>/N<sub>2</sub> = 65/25/5/5 [27]

**Figure 3** Pore size distributions of the CeO<sub>2</sub> support and the fresh Pd/CeO<sub>2</sub> powder calculated from N<sub>2</sub> adsorption data using the Barrett-Joyner-Halenda method.

**Figure 4** XRD diffractograms of the CeO<sub>2</sub> support and the Pd/CeO<sub>2</sub> powders before and after testing in FBR.

**Figure 5** Bright-field TEM micrographs of the fresh Pd/CeO<sub>2</sub> powder at different magnifications.

**Figure 6** Dark-field STEM micrograph (a) and complementary EDS Ce (b), Pd (c), and O (d) mapping of the fresh Pd/CeO<sub>2</sub> powder.

**Figure 7** Dark-field STEM micrograph and complementary EDS Ce (b), Pd (c), and O (d) mapping of the used Pd/CeO<sub>2</sub> powder.

**Figure 8** SEM pictures of the fresh Pd/CeO<sub>2</sub> coated foil at low (a) and high (b) magnification.

**Figure 9** SEM pictures of the fresh (a-b) and the used (c-d) Pd/CeO<sub>2</sub> coated foil at 10<sup>4</sup>-10<sup>5</sup> magnification.

**Figure 1**

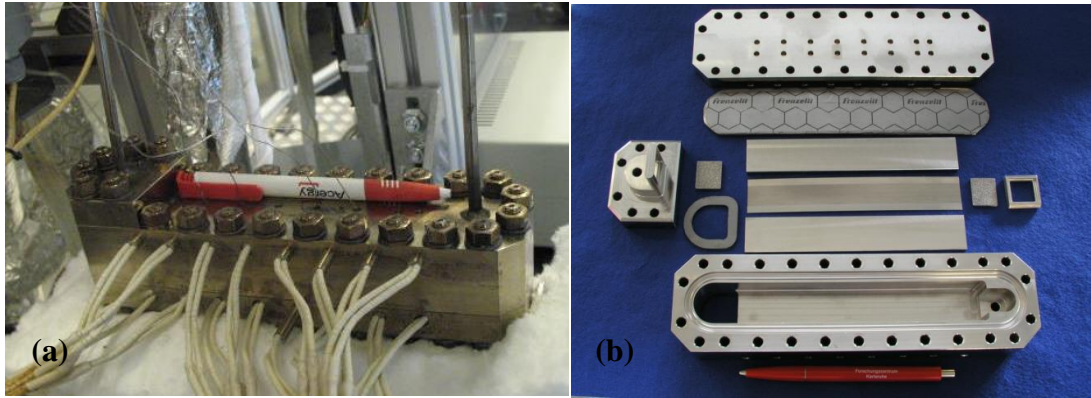
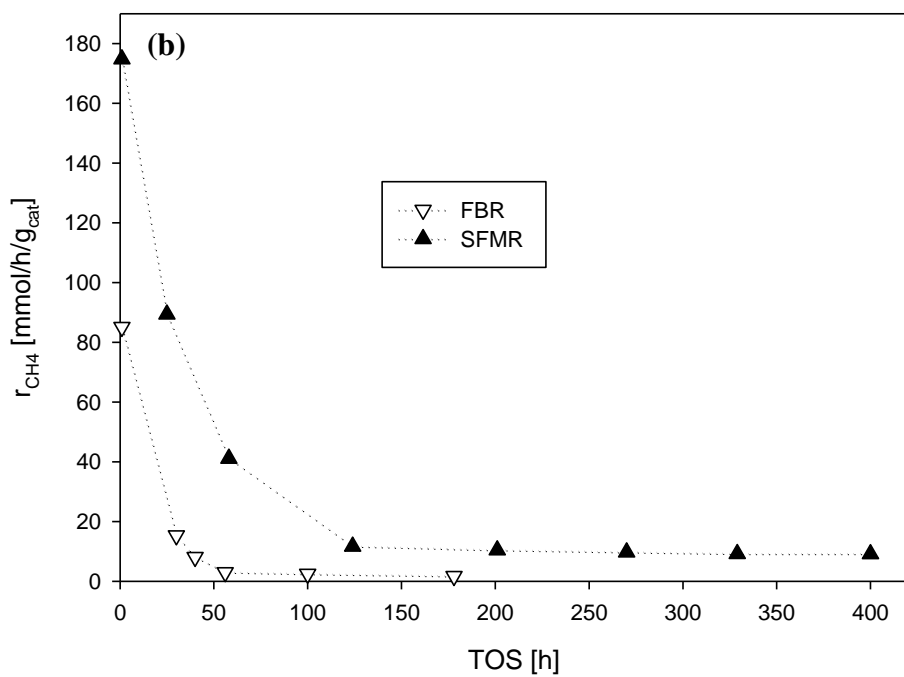
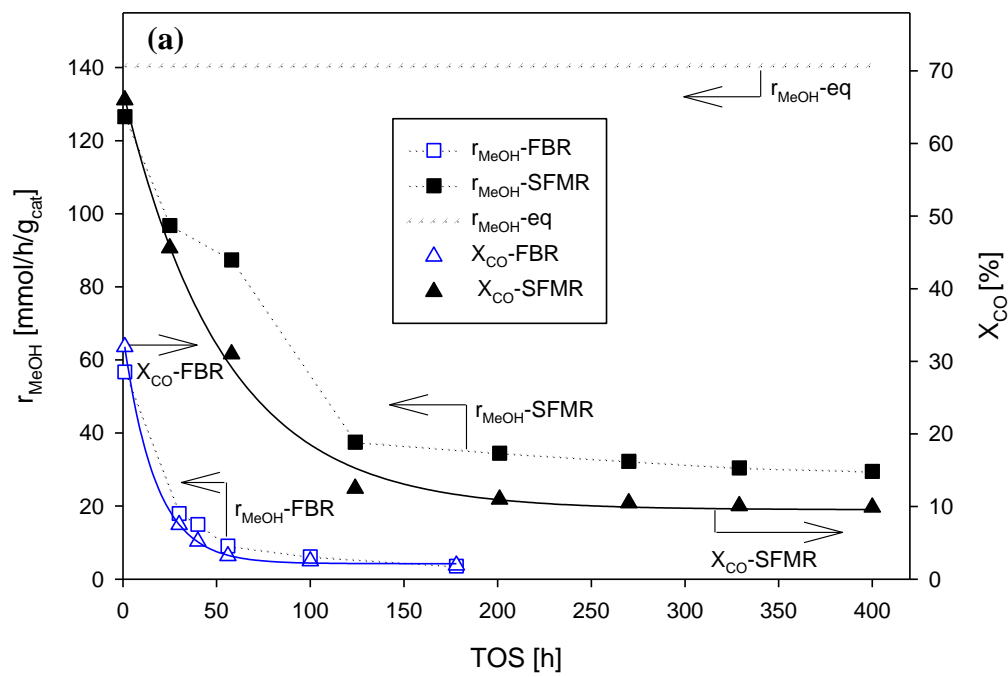


Figure 2



**Figure 3**

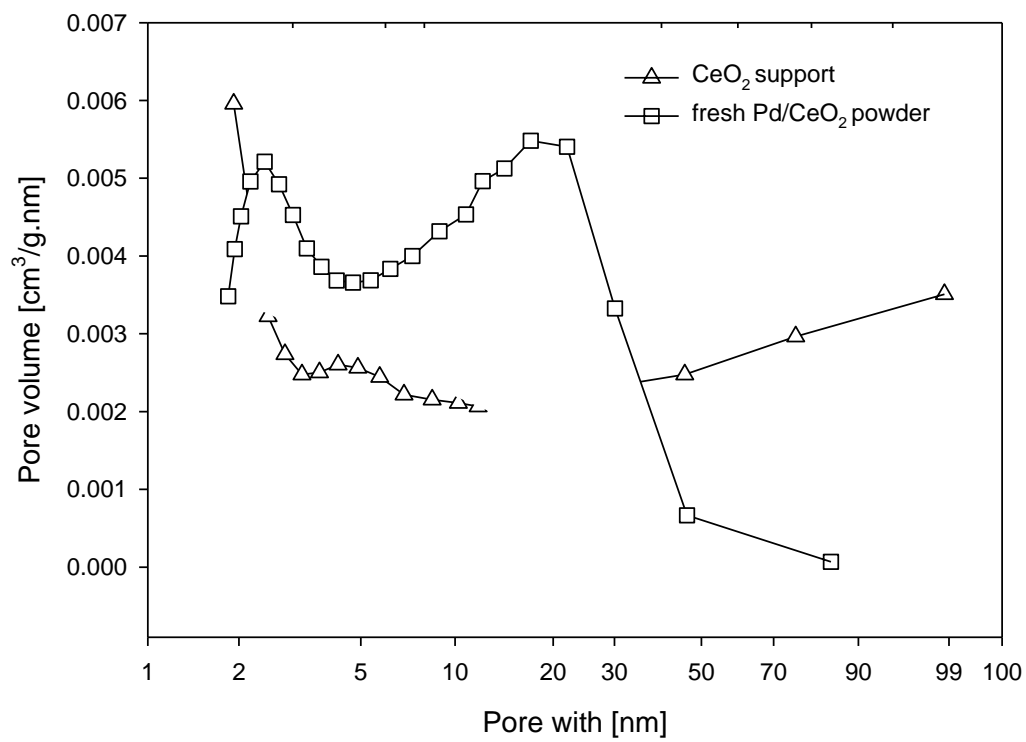
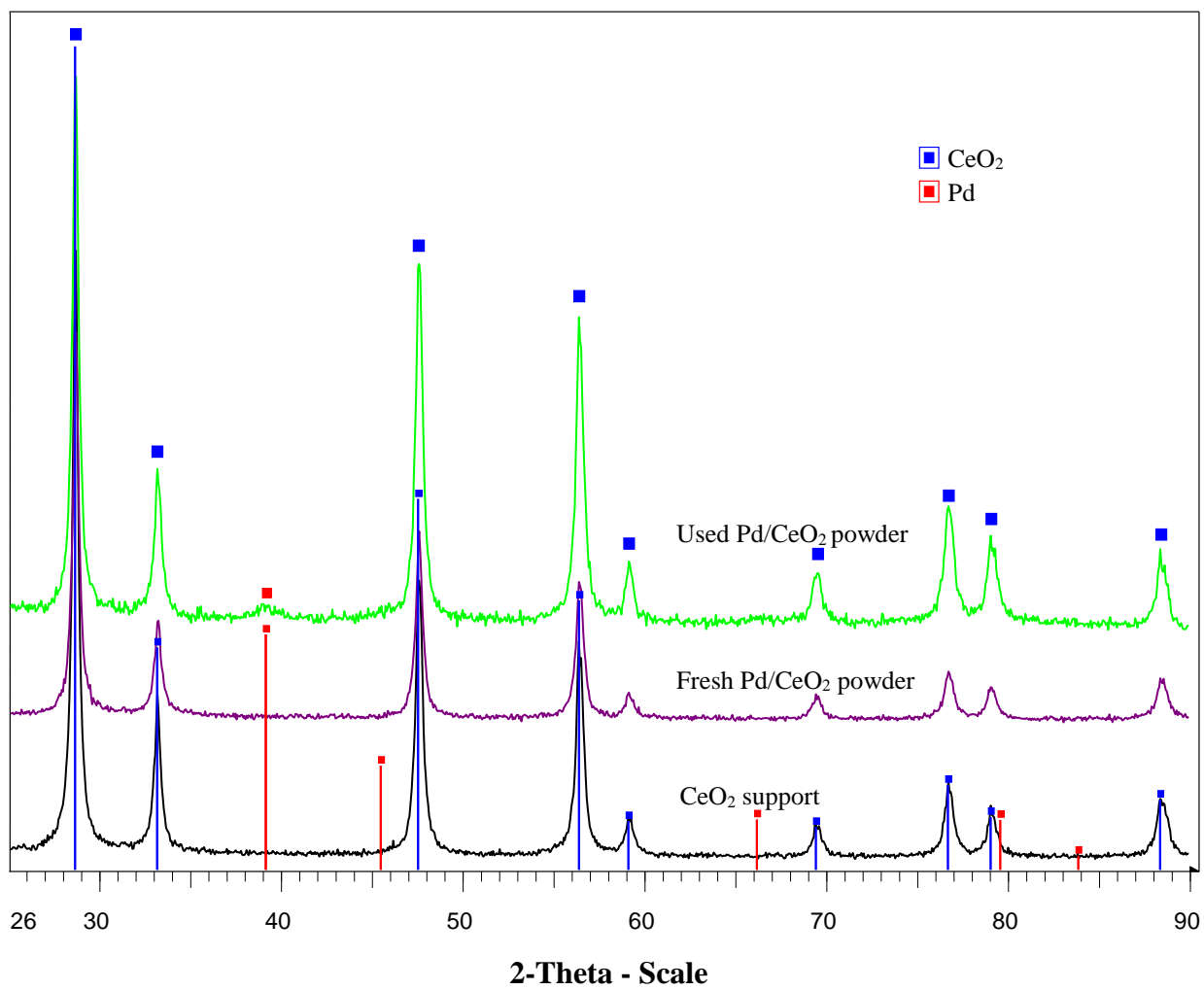
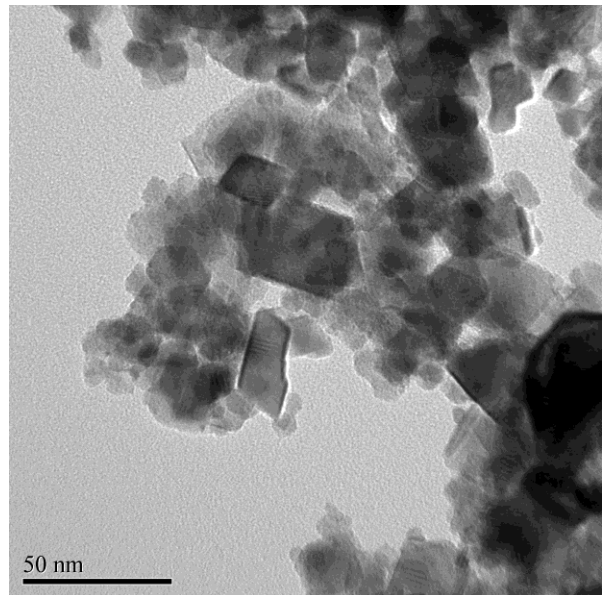
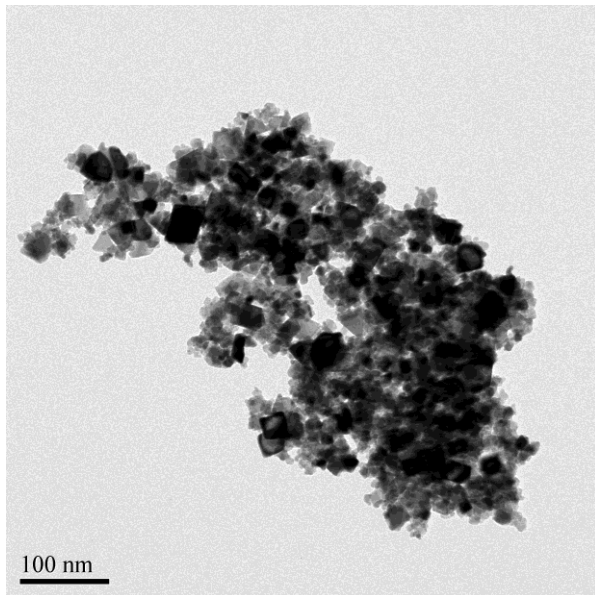


Figure 4



**Figure 5**



**Figure 6**

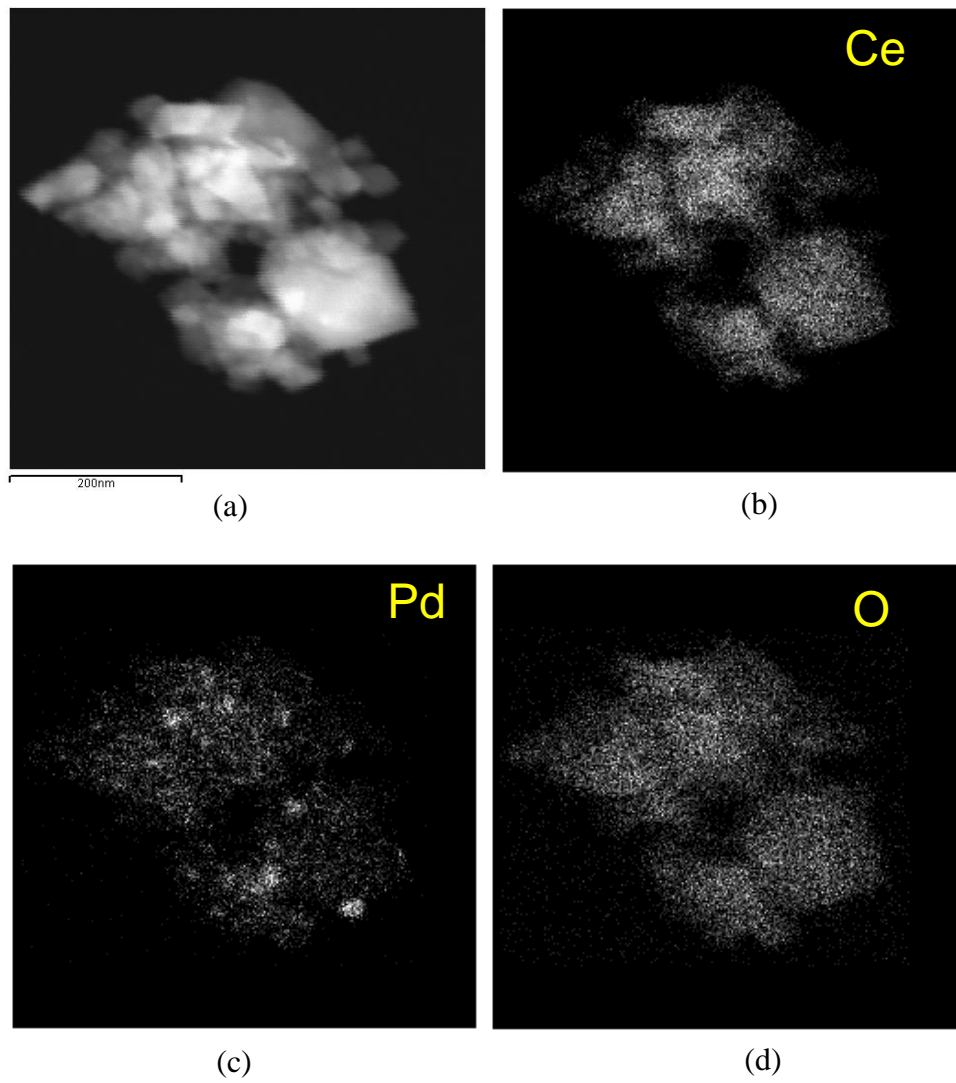


**Figure 7**

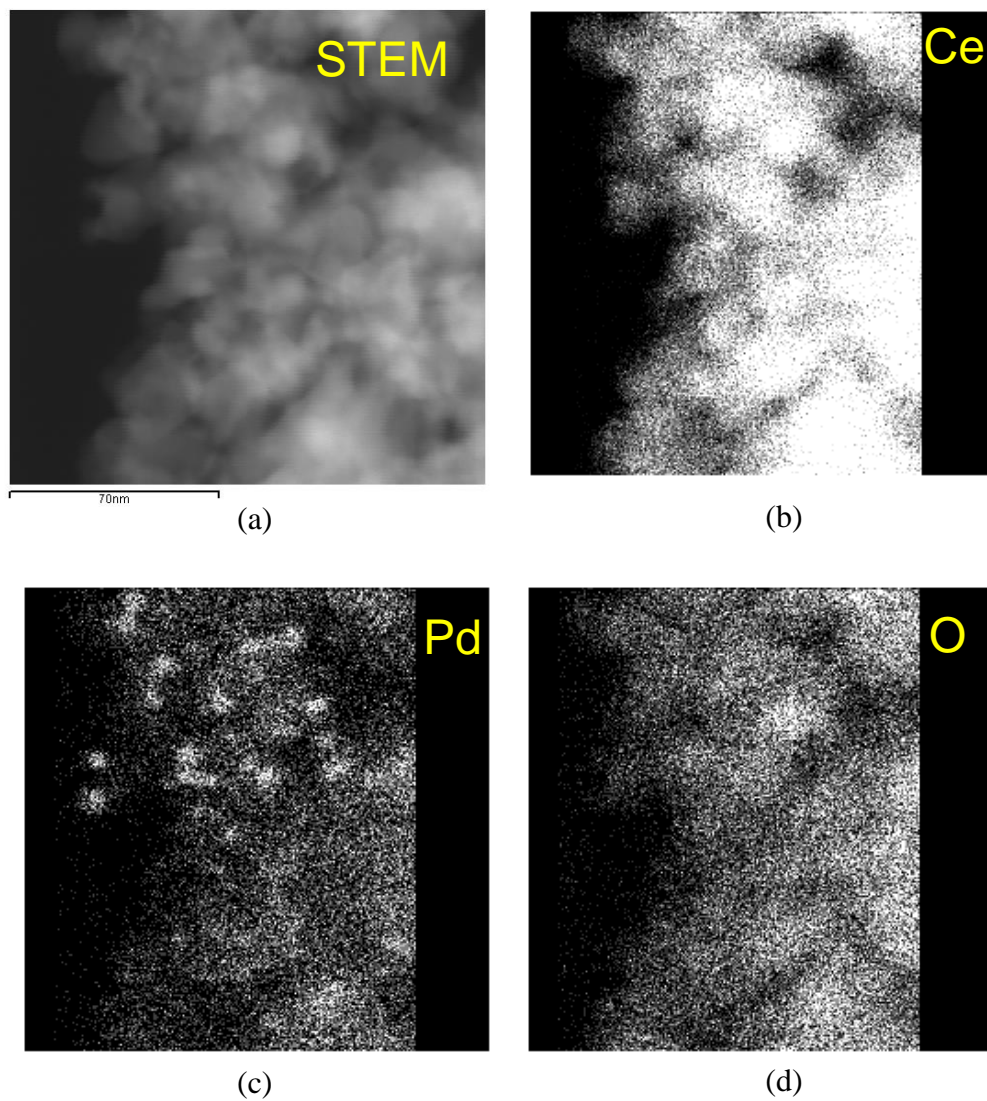
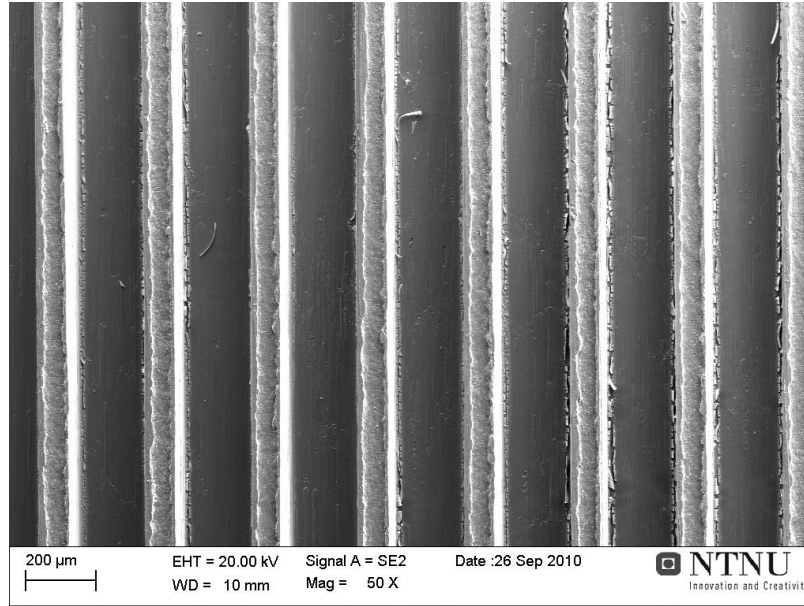
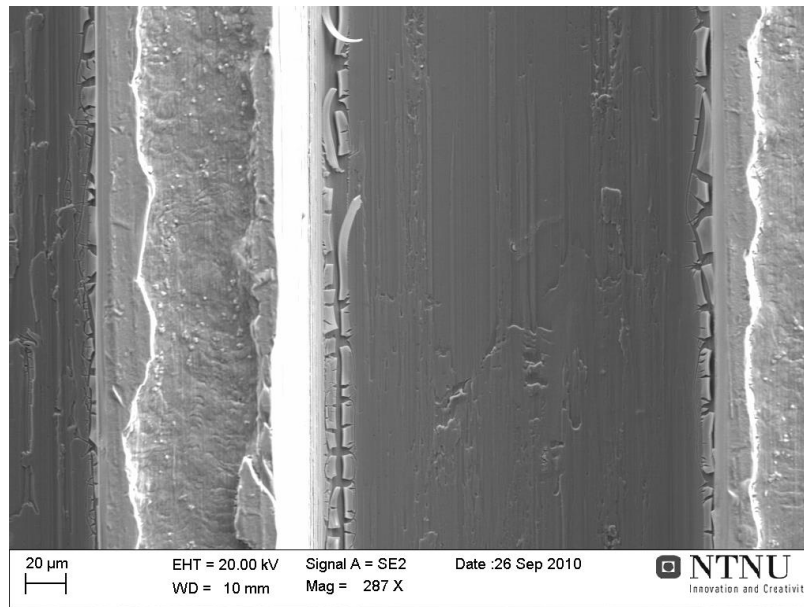


**Figure 8**

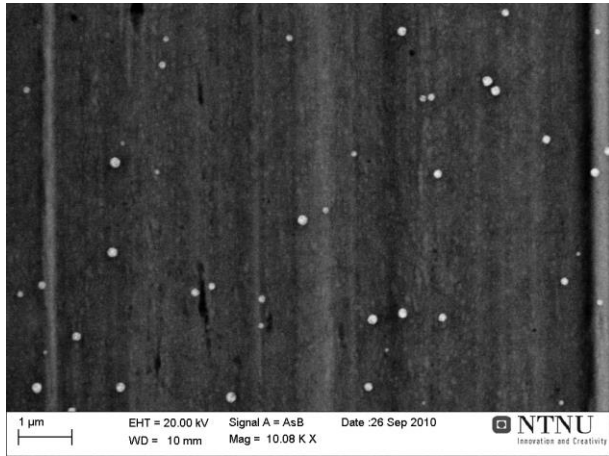


(a)

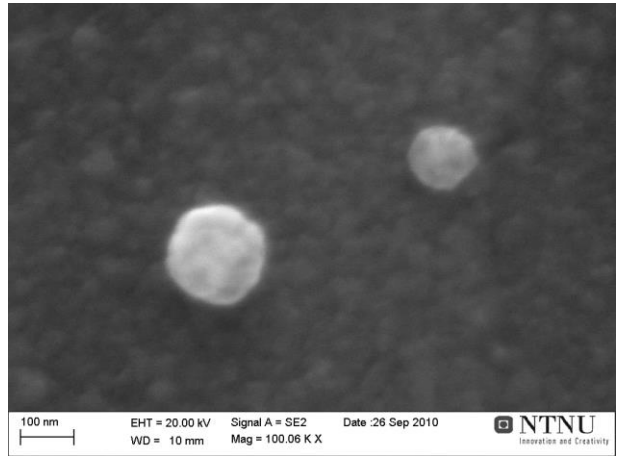


(b)

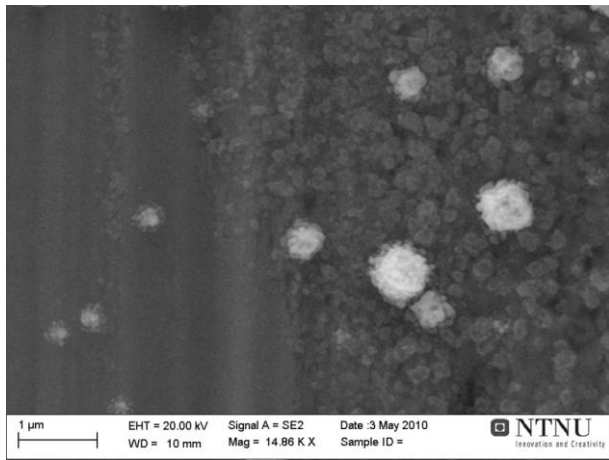
Figure 9



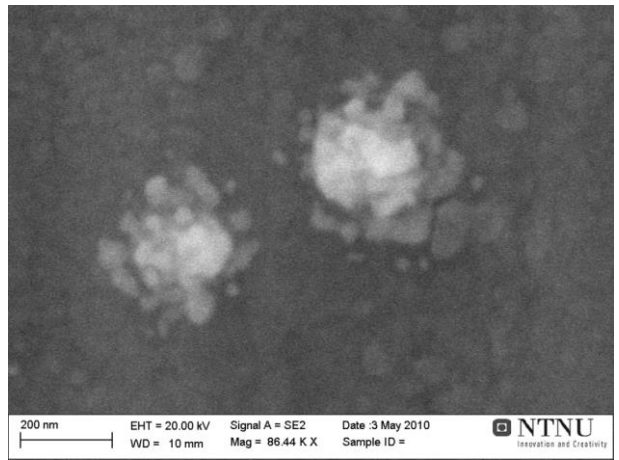
(a)



(b)



(c)



(d)

**Table 1** Characterization of the CeO<sub>2</sub> nanoparticle support and the fresh Pd/CeO<sub>2</sub> powder catalyst

	S <sub>BET</sub> [m <sup>2</sup> /g] <sup>a</sup>	d <sub>pore</sub> [nm] <sup>b</sup>	Pore volume [cm <sup>3</sup> /g] <sup>b</sup>	D [%] <sup>c</sup>	dp [nm] <sup>d</sup>
CeO <sub>2</sub>	32	21	0.178	-	-
Pd/CeO <sub>2</sub>	52	14	0.183	32	3.4

<sup>a</sup> BET surface area.

<sup>b</sup> Average pore size and pore volume calculated by using BJH method.

<sup>c</sup> Pd dispersion calculated from CO chemisorption at 313 K.

<sup>d</sup> Pd particle size based on CO chemisorption at 313 K.